# Large-eddy simulations on pollutant reduction effects of road-center hedge and solid barriers in an idealized street canyon

Chao Lin, Ryozo Ooka, Hideki Kikumoto, Cédric Flageul, Youngseob Kim, Yunyi Wang, Alice Maison, Yang Zhang, Karine Sartelet

# Large-eddy simulations on pollutant reduction effects of road-center hedge and solid barriers in an idealized street canyon

Chao Lin [a,*], Ryozo Ooka [a], Hideki Kikumoto [a], Cédric Flageul [b], Youngseob Kim [c], Yunyi Wang [c], Alice Maison [c,d], Yang Zhang [e], Karine Sartelet [c]

[a] Institute of Industrial Science, The University of Tokyo, 4-6-1 Komaba, Meguro-ku, Tokyo 153-8505, Japan

[b] Curiosity Group, Pprime Institute, Université de Poitiers, CNRS, ISAE-ENSMA, Chasseneuil, France

[c] CEREA, École des Ponts ParisTech, EdF R&D, IPSL, 77 455 Marne la Vallée, France

[d] Université Paris-Saclay, INRAE, AgroParisTech, UMR EcoSys, 91120 Palaiseau, France

[e] Department of Civil and Environmental Engineering, Northeastern University, Boston, MA 02115, USA

[*] Corresponding author, c-lin415@iis.u-tokyo.ac.jp

Highlight

- The road-center barriers reshaped the vortices in an idealized street canyon.
- The barriers reduced concentrations in the perpendicular and oblique wind directions.
- The barriers enhanced the vertical pollutant removal at the top of the street canyon.
- Larger barriers' width and the hedge's leaf area density decreased near-wall concentration.
- The relative effectiveness of hedge and solid barriers varied with wind directions.

Abstract

This study conducted large-eddy simulations (LES) on the pollutant reduction effects of hedge and solid barriers in a three-dimensional idealized street canyon with an aspect ratio of 0.5. The wind direction was perpendicular and oblique (45 degrees) to the street. The results were validated with data from wind tunnel experiments. LES accurately predicted the concentration distribution in the barrier-free case and reproduced well the barrier-induced concentration reduction. In the barrier-free case, a large recirculation vortex was observed. However, the central barriers forced the recirculated airflow in the middle of the canyon and newly formed vortices near the leeward walls. The two counter-direction vortices in the hedge and solid barrier cases transported pollutants toward the center of the canyon and enhanced the vertical pollutant removal at the top of the street canyon. The hedge barrier (solid barrier) reduced spatially-averaged concentration by about 59% (45%) near the leeward wall, 64% (20%) near the windward wall, and 45% (17%) in the whole street canyon compared to the barrier-free case. The effects of leaf area density (LAD) and barrier width were further investigated under the perpendicular wind direction.

Increasing the LAD or the width of the hedge barrier decreased concentration near the leeward walls but increased canyon-averaged concentration. Increasing the width of the solid barrier decreased the concentration near the leeward walls and the canyon-averaged concentration. In an oblique wind direction, the hedge and solid barriers reduced by about 30% and 60% the spatially-averaged concentration near the building walls compared to the barrier-free case.

Keywords
Pollutant dispersion, Street canyon, LES, Barrier, Vegetation

## 1 Introduction

Outdoor air pollution is an important environmental problem in the urban environment [1] and poses a major long-term health risk of respiratory diseases [2]. Vehicular emissions are the predominant source of air pollution in streets [3]. Three main approaches are considered to mitigate air pollution, including (i) controlling the activity (e.g., the number of cars), (ii) controlling the emission intensity (e.g., reducing emission factors), and (iii) controlling source-receptor pathways [4]. Among them, controlling source-receptor (traffic emissions-roadside residences) pathways has been considered as a low-cost passive method for existing streets compared to the other two methods which take a long time to achieve [5,6].

Road barriers have been identified as effective passive methods to control source-receptor pathways and reduce personal exposure in open roads and street canyons [7]. Road barriers can be divided into porous barrier and solid barrier [8]. Hedges are common porous barriers and are low-level vegetation with continuous leaves covering from the ground to the top. Hedges can act either partially or completely as a baffle between traffic emissions and roadside receptors [9]. On the other hand, solid barriers, including low boundary walls [10] and noise barriers [11,12], act as baffle plates and redirect the flow and thereby affect the dispersion at street level. The essential difference between hedge barriers and solid barriers is that the wind can pass through the hedge barriers at a reduced wind speed depending on the porosity, whereas the wind is forced over the solid barrier. Reducing the porosity (or increasing the density) of hedge barriers may make their effect close to that of solid barriers.

The pollutant reduction effect of hedge and solid barriers in street canyons is largely dependent on their proper implementation. Several common considerations have been recommended for both hedge and solid barriers. For instance, Gallagher et al. [13] and Gromke et al. [14] reported that one central barrier resulted in greater improvements in pollutant concentration reduction than two sidewise barriers. In addition, increasing the barrier height was found resulting in more

effective pollutant reduction near the building walls [14,15]. Moreover, the barrier effects are also dependent on the wind direction. McNabola et al. [10] reported that the solid barriers reduced the pollutant exposure of pedestrians walking on sidewalks by up to 40% and 75% under perpendicular and parallel wind conditions, respectively.

To reduce construction and maintenance costs, the barrier width is expected to be as thin as possible. Tong et al. [16] showed that increasing hedge barrier width resulted in a greater reduction in concentration behind the barrier in an open road situation. However, the influence of barrier width for both hedge and solid barriers in a street canyon is unclear. In addition, the density or leaf area density (LAD) is an important parameter for vegetation [17,18]. The LAD of hedges is generally higher than that of tree crowns [19]. Gromke et al. [14] reported that increasing hedge density resulted in a concentration decrease near the building walls. However, as a LAD increase also leads to a wind velocity decrease [20], the ventilation rate of the street canyon could decrease. Therefore, further investigations are needed to find out how hedge LAD affects the flow and concentration fields in a street canyon.

Among the methods of studying the effect of hedge and solid barriers in street canyons, on-site monitoring (field measurement), wind tunnel experiment (reduced scale experiment) and numerical modeling (analytical model and computational fluid dynamics) are frequently adopted. On-site monitoring can provide knowledge of the barrier effect in real-world situations [21–24]. Wind tunnel experiments use real fluids to accurately reproduce flows and allow systematic investigations [14]. However, these methods are high-cost and can only provide limited information on complicated flow and concentration fields. With the development of numerical simulations, computational fluid dynamics (CFD) simulation has been widely used to simulate dispersion in street canyons. A commonly adopted method involves conducting CFD simulations after validating an experimental value. In the CFD technique, Reynolds-averaged Navier-Stokes (RANS) models [15] and large-eddy simulation (LES) [5,10,13] are frequently used to represent for barrier effects. In urban environments with complicated flow fields, LES has shown more accurate prediction accuracy on airflow and pollutant dispersion than the RANS model [25,26]. However, few studies have been reported to perform CFD simulations using LES on hedge and solid barriers effects in a street canyon and validate the accuracy using experimental values.

In this study, we conducted LES to estimate the pollutant reduction effect of hedge and solid barriers in a street canyon. The accuracy of LES on the concentration field was validated by wind tunnel experiments [14,27]. Moreover, we investigated the influences of LAD and barrier width. The above studies were based on a wind direction which was perpendicular (90 degrees) to the

street. Additionally, the barrier effects were evaluated under an oblique wind direction which was 45 degrees to the street.

The remainder of this paper is organized as follows. In Section 2, the simulation settings are described, including street configuration, numerical methods of flow and dispersion modeling, and modeling of hedge barrier and analysis cases. In Section 3, the simulation results are validated against a wind tunnel database. The flow and concentration fields of the barrier-free, hedge barrier and solid barrier cases are presented to investigate the effect of the presence of barriers. The influence of LAD, barrier widths, and wind directions are then analyzed. Finally, conclusions and perspectives are presented in Section 4.

## 2 CFD simulation settings

### 2.1 Street canyon configuration, computational domain and grids

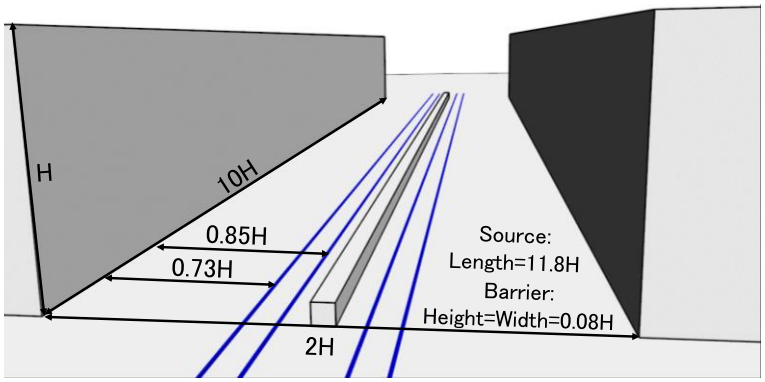


Fig. 1. Schematic of the wind tunnel geometry [14].

The simulated results were validated against the wind tunnel dataset [14,27], where the detailed description of the wind tunnel experiment can be found. Gromke and Ruck (2012) [27] provided concentration distributions of the barrier-free case near the leeward and windward walls of the street canyon. In addition, Gromke et al. (2016) [14] provided concentration measurement data of street canyons with hedge and solid barriers. The street canyon configuration (Fig. 1) was set according to the full-scale model represented by the wind tunnel model. The length scale between the wind tunnel and the full-scale models was 1:150. The building height $H$ of the isolated street canyon was 18 m. The width and length of the street canyon were $2H$ and $10H$, respectively. The aspect ratio of the street canyon was 0.5. The barrier models and line sources were placed along the street. The line sources exceeded the street canyon by about $1H$ on each side to represent the traffic emission in the intersections. The barriers were located at the center of the canyon, and the height and width of the barriers were considered as $0.08H$ (1.5 m) based on the wind tunnel experiment [14].

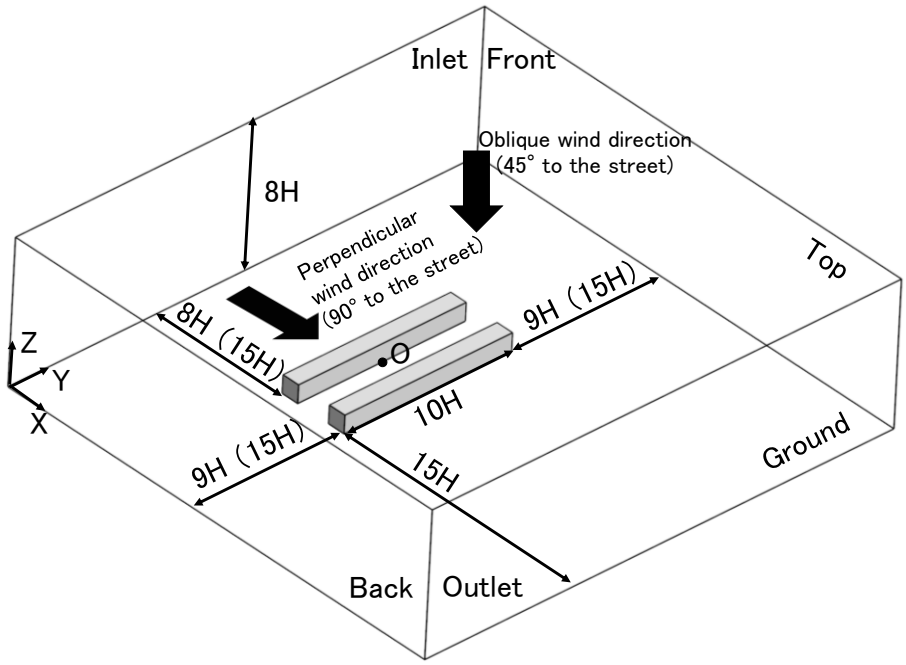


Fig. 2. Simulation domain. The values in parentheses denote domain size in the oblique wind direction cases.

Fig. 2 shows the simulation domain. $x$, $y$ and $z$ represent the streamwise, spanwise and vertical directions, respectively. The height of the domain was set to 8$H$. The distances from the buildings to the boundaries were based on the Architectural Institute of Japan (AIJ) guidelines [28]. The distance between the outlet boundary and the downwind building was 15$H$. For perpendicular wind cases, the distance between the inlet boundary and the front face of upwind building was 8$H$, and between the lateral boundaries and the buildings were 9$H$. For oblique wind cases, a larger simulation domain was set. The distance between the inlet boundary and the front face of upwind building was 15$H$, and between the lateral boundaries and the buildings were 15$H$. As shown in Fig. 3, the simulation domain was discretized into hexahedral cells. Based on the preliminary grid sensitivity check outlined in Appendix A, the total grid number was set to approximately 1.5 million. The smallest and largest grid sizes in the street canyon were 0.014$H$ and 0.056$H$, respectively.

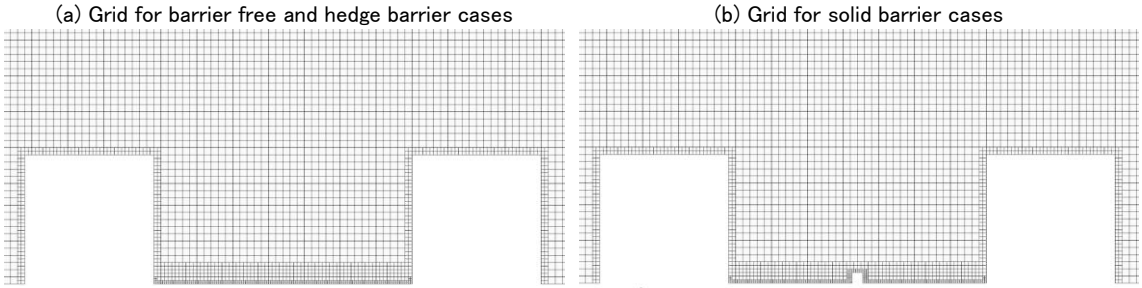


Fig. 3. Grid resolutions in the street canyon.

2.2 Numerical methods and boundary conditions

The transport equations for momentum and concentration for LES can be referred in previous studies [29,30]. The open-source CFD software OpenFOAM v2012 [31] was used. For the turbulence model, the wall-adapting local eddy-viscosity (WALE) model [32] was chosen because it can correctly reproduce the turbulence scaling near the wall without using a damping function. The WALE model was used successfully in the flow and concentration fields in complex urban geometries [33,34]. The momentum and concentration equations were discretized using the total variation diminishing (TVD) scheme [35,36], which combines the first-order upwind difference scheme and the second-order central difference scheme. The PIMPLE algorithm, a merged PISO (Pressure Implicit with Splitting of Operator)–SIMPLE (Semi-Implicit Method for Pressure-Linked Equations) algorithm in the OpenFOAM toolkit, was used for pressure–velocity coupling. The sub-grid scale Schmidt number was set to 0.5 [37]. The time step was set to $\Delta t = 0.1$ s $(0.026H/U_H)$. The computation was performed for 3600 s before being time-averaged for 3600 s $(930H/U_H)$. The time-averaged streamwise velocity $U$ at building height $H$ was $U_H = 4.65\ m/s$. The sampling time was considered sufficient to obtain the time-averaged and fluctuation values.

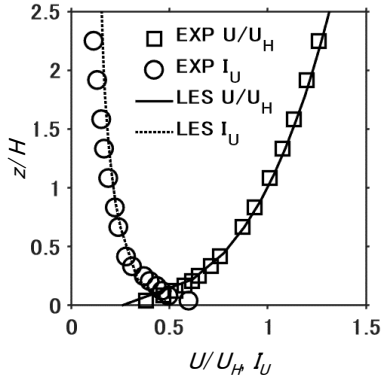


Fig. 4. Time-averaged streamwise velocity $U$ and turbulence intensity $I_U$ in streamwise direction of inflow. $U_H$ and $I_{U,H}$ were the time-averaged streamwise velocity $U$ and turbulent intensity $I_U$ at building height $H$.

The inlet boundary conditions (Fig. 4) were set according to the wind tunnel experiments to reproduce the atmospheric boundary layer. The turbulent intensity $I_U$ at building height $H$ was $I_{U,H} = 0.19$. The vertical profiles of $U$ and $I_U$ can be described by power law formulations as follows:

$$U(z) = U_H(z/H)^{\alpha_U} \quad (1)$$

$$I_U(z) = I_{U,H}(z/H)^{\alpha_I} \quad (2)$$

where power law exponents for $U$ and $I_U$ were $\alpha_U = 0.3$ and $\alpha_I = 0.36$, respectively. In LES, the digital-filter method [38] was used to generate synthetic turbulence at the inlet boundary. The Reynolds stresses and turbulent length scale were approximated from the experiment [39]. For the outlet boundary conditions, the pressure and the gradients of all other variables were set to zero. Slip boundary conditions were used for the top boundary. No-slip boundary conditions based on Spalding's law [40] were prescribed at ground and building surfaces. The lateral boundaries (front and back) were considered as symmetric in the perpendicular wind cases, and as inlet and outlet in the oblique wind cases. The pollutant was emitted using source term in the concentration transport equation with a source intensity of one. The concentration at the inlet was set to 0. The concentration results were presented in nondimensionalized values. The nondimensionalized instantaneous concentration $c$ was calculated from $c = c_{raw}/c_{ref}$, where $c_{raw}$ was the computed concentration and $c_{ref} = (Q/L)/(U_H H)$ was the reference concentration. $Q/L$ was the emission rate per unit length of the source. The nondimensionalized time-averaged concentration and nondimensionalized concentration fluctuation were indicated as $C$ and $c'$.

2.3 Modelling of hedge barrier

To reproduce the aerodynamic effect of the hedge barrier, a source term was assigned to the momentum transport equation [41]. Assuming the form drag was much larger than the viscous drag, the momentum source term of tree canopy was modelled as follows:

$$S_{u_i} = -C_D \mathrm{LAD} u_{mag} u_i \quad (3)$$

where $u_{mag}$ was the velocity magnitude, $u_i$ was the velocity component in the $i$-th direction, and $C_D$ was the dimensionless drag coefficient. In the wind tunnel experiment [14], the hedge barrier was modelled by using porous media with different porosities. The porosity was described by pressure loss coefficient $\lambda$, given by

$$\lambda = 2C_D \mathrm{LAD} \quad (4)$$

and $\lambda$ was measured by

$$\lambda = \frac{\Delta p_{st}}{0.5\rho u^2 d} \quad (5)$$

where $\Delta p_{st}$ was the difference in static pressure between the windward and leeward of the porous media, $0.5\rho u^2 d$ was the dynamic pressure, $d$ was the porous foam sample thickness in the streamwise direction. Measurements of $\lambda$ resulted in 250 $\mathrm{m}^{-1}$ for the wind tunnel scale, representing $\lambda = 1.67\ \mathrm{m}^{-1}$ in the full scale. By considering $C_D = 0.2$ [42], LAD $= 4.2\ \mathrm{m}^2/\mathrm{m}^3$ can be interpreted from $\lambda$. Although the hedge influence on the flow turbulence was not considered in the previous LES studies on the pollutant dispersion in street canyons, the LES showed accurate accuracy with wind tunnel experiments [41,43]. The reason could be that most of turbulent kinetic energy was solved at the resolved scale. In this study, over 95% of turbulent kinetic energy was solved at the resolved scale as shown in Fig. A4 in Appendix A. Therefore, neglecting the sink or source terms for turbulence was considered acceptable in this study. In accordance with the experiment, the deposition effect of the hedge barrier was not considered. Meanwhile, it should be noted that the deposition velocity is largely different depending on the pollutant species, especially for the particles [44]. Therefore, this study targeted on the gaseous species with small deposition velocities such as carbon monoxide and nitrogen oxides [45].

## 2.4 Analysis cases

Table 1 shows the description of barrier configurations for all analysis cases. Cases were formulated by considering the influence of LAD, barrier width and wind direction. For the basic cases which corresponded to the experiment configurations, the simulated time-averaged concentration was validated using experimental data in Section 3.1 and the pollutant reduction effect from hedge and solid barriers were investigated in Section 3.2. Next, the influence of hedge porosity was analysed by considering successively the LAD as 1 and 2 $\mathrm{m}^2/\mathrm{m}^3$ [19] in Section 3.3. Then, hedge and solid barriers with smaller width (1 m and 0.5 m) were considered in Section 3.4. Subsequently, wind direction was considered as 45° in Section 3.5. Other configurations were the same as in the basic cases.

Table 1. Description of barrier configurations for all analysis cases.

| Barrier | LAD ($\mathrm{m}^2/\mathrm{m}^3$) | Width (m) | Wind direction (°) | Note |
|---|---|---|---|---|
| Basic cases[a] | | | | |
| Free | N/A | N/A | | Section 3.1 |
| Hedge[b] | 4.2 | 1.5 | 90 | Section 3.2 |
| Solid | N/A | 1.5 | | Section 3.3 |
| Discussion on LAD | | | | |
| Hedge | 1.0, 2.0, 4.2 | 1.5 | 90 | Section 3.4 |
| Discussion on barrier width | | | | |

| | | | | |
|---|---|---|---|---|
| Hedge | 4.2 | 0.5, 1.0, 1.5 | 90 | Section 3.5 |
| Solid | N/A | 0.5, 1.0, 1.5 | | |
| Discussion on wind direction | | | | |
| Free | N/A | N/A | | |
| Hedge | 4.2 | 1.5 | 45 | Section 3.6 |
| Solid | N/A | 1.5 | | |

[a] The results of basic cases were validated with wind tunnel experiments.

[b] The dimensionless drag coefficient $C_D = 0.2$.

## 3 Results and discussions

### 3.1 Validation on the time-averaged concentration in the basic cases

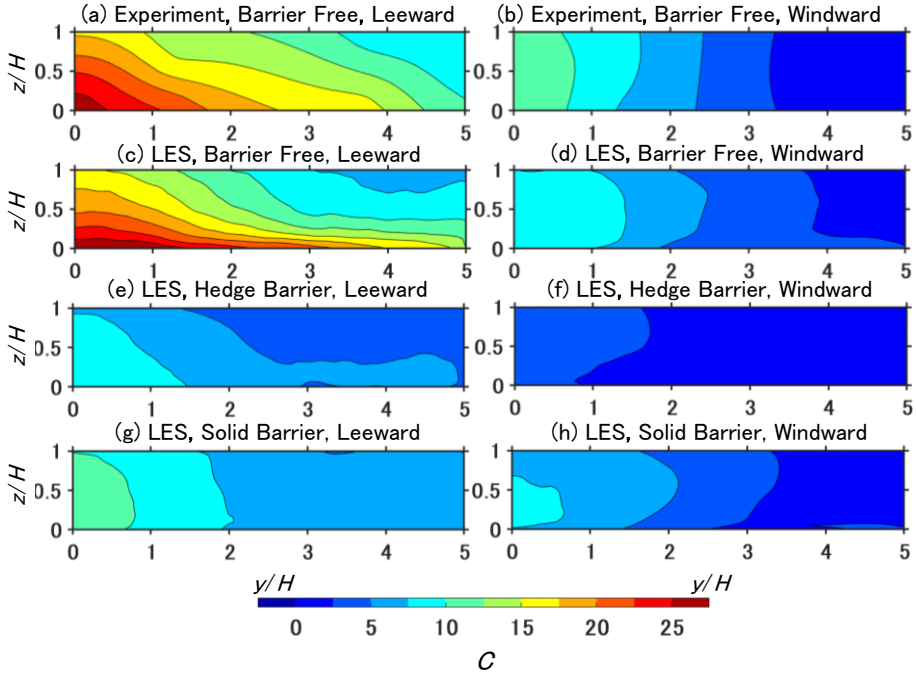


Fig. 5. Distributions of the time-averaged concentration $C$ near the leeward wall ($x/H$=0.06) and the windward wall ($x/H$=1.94) in the basic cases. The experiment data is from Gromke and Ruck (2012) [27].

In the Sections 3.1 to 3.4, the studies were based on a wind direction which was perpendicular (90 degrees) to the street. Fig. 5 shows the distributions of the time-averaged concentration $C$ near the leeward wall ($x/H$=0.06) and the windward wall ($x/H$=1.94) in the basic cases (barrier-free, hedge barrier with LAD=4.2 $m^2/m^3$ and solid barrier). The vertical planes were selected with the same location in the wind tunnel experiment [27]. As the simulation configurations were symmetric in the spanwise direction, the simulation results were averaged at mirror-symmetric locations. The simulation results were confirmed to be symmetrical in the spanwise direction in Appendix B. All subsequent results were presented using the same methods. The barrier-free case

was validated by the experimental data [27]. Although the simulated $C$ values were smaller than the experiment, LES well reproduced the distribution patterns for both leeward and windward sides. In all cases, the $C$ values near the leeward walls were larger than those near the windward walls. In addition, the hedge and solid barriers largely reduced time-averaged concentration from the barrier-free case, indicating that barriers were effective methods for reducing roadside pollutants. The detailed analysis can be found in Section 3.2.

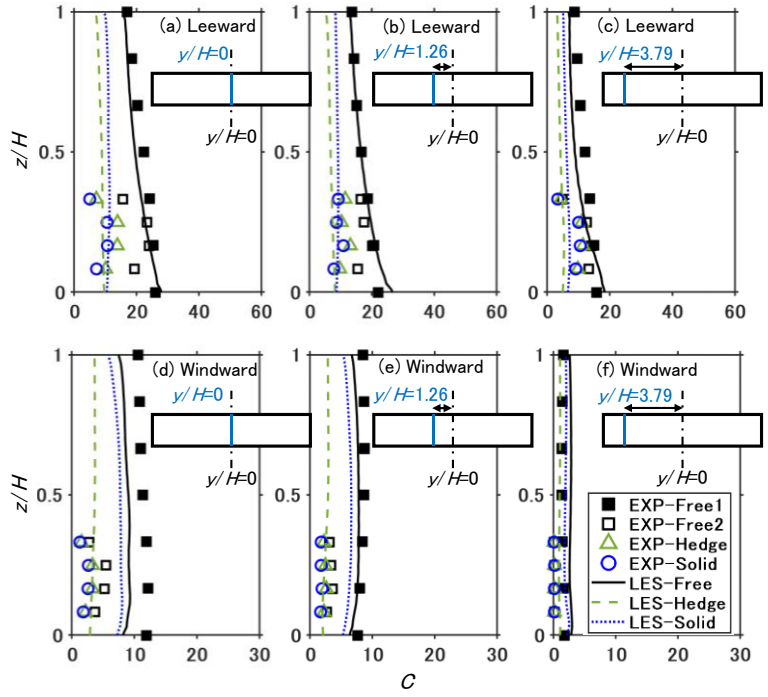


Fig. 6. Vertical profiles of the time-averaged concentration near the leeward wall ($x/H$=0.06) and the windward wall ($x/H$=1.94) in the basic cases. EXP-Free1 indicates the experimental data from Gromke and Ruck (2012) [27]. Other experimental data are taken from Gromke et al. (2016) [14].

Fig. 6 shows the vertical profiles of the time-averaged concentration $C$ near the leeward wall ($x/H$=0.06) and the windward wall ($x/H$=1.94). The barrier-free data obtained in the wind tunnel experiments conducted by Gromke and Ruck (2012) [27] and Gromke et al. (2016) [14] were shown together. The two datasets showed similar values near the leeward wall, while discrepancy was found near the windward wall. In addition, the hedge and solid barriers showed similar concentration reduction in Gromke et al. (2016) [14]. Regarding the LES prediction for the barrier-free case, LES was in good agreement with Gromke and Ruck (2012) [27] on both sides of the street canyon. Furthermore, both experiment and LES showed that the concentration values in the hedge and solid barrier cases were lower than those in the barrier-free cases, indicating that LES well reproduced the barrier-induced pollutant reduction.

277 3.2 Flow and concentration fields of basic cases

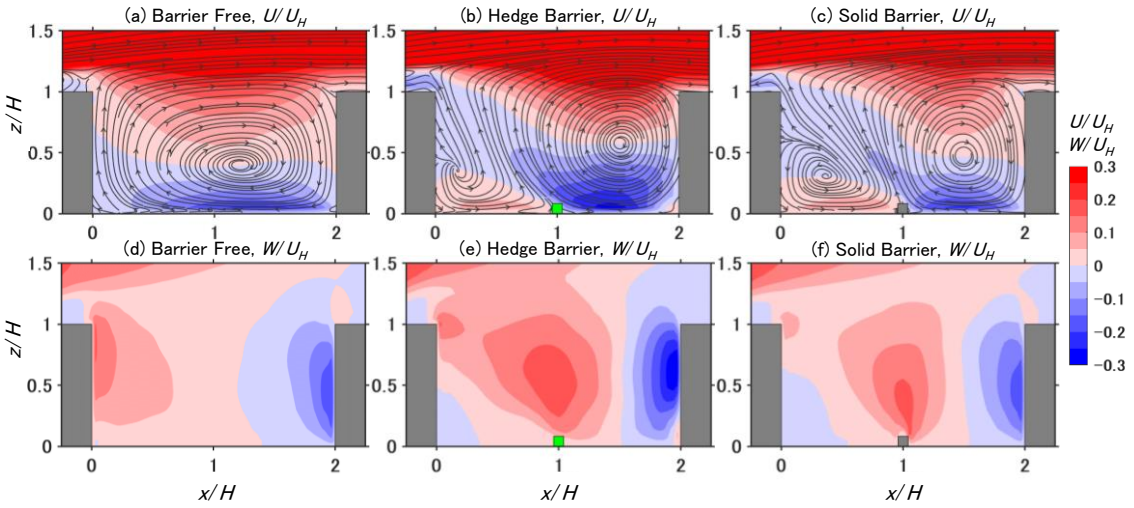


278

279 Fig. 7. Distributions of the time-averaged streamlines, streamwise velocity $U/U_H$ and vertical
280 velocity $W/U_H$ in the vertical plane ($y/H$=0).

281

282 To find out how barriers affected the flow field in the street canyon,
283 Fig. 7 shows the distributions of the time-averaged streamlines, streamwise velocity $U/U_H$ and
284 vertical velocity $W/U_H$ in the vertical plane ($y/H$=0) in the basic cases (barrier-free, hedge barrier
285 with LAD=4.2 $m^2/m^3$ and solid barrier). In the barrier-free case, a large recirculation vortex can
286 be found in the street canyon. Meanwhile, the presence of barriers forced the recirculated air flow
287 up at the middle of the canyon ($x/H$=1) and newly formed the vortices between the leeward walls
288 and the barriers, which was also observed in a street canyon with an aspect ratio of 0.75 in
289 McNabola et al. (2009) [10]. The new vortices were referred as leeward vortices hereafter, to be
290 distinct from the original vortices which were referred to as windward vortices. In both hedge and
291 solid barrier cases, the leeward vortices were in counter rotation direction with the windward
292 vortices. In addition, the windward vortices were larger than the leeward vortices. At the same
293 time, the hedge barrier case showed a stronger windward vortex compared to the solid barrier
294 case. This can be attributed to the fact that the recirculated air flow was able to pass through the
295 permeable hedge barrier but was forced over the solid barrier. Consequently, a stronger leeward
296 vortex was formed in the solid barrier case than in the hedge barrier case. In addition, although
297 the hedge barrier case generally showed larger $W/U_H$ than the solid barrier case in the street
298 canyon, the solid barrier case showed larger $W/U_H$ than the hedge barrier case close to the solid
299 barrier. The effect of the porosity or LAD of hedge barriers on the flow fields is further discussed
300 in Section 3.3.

301

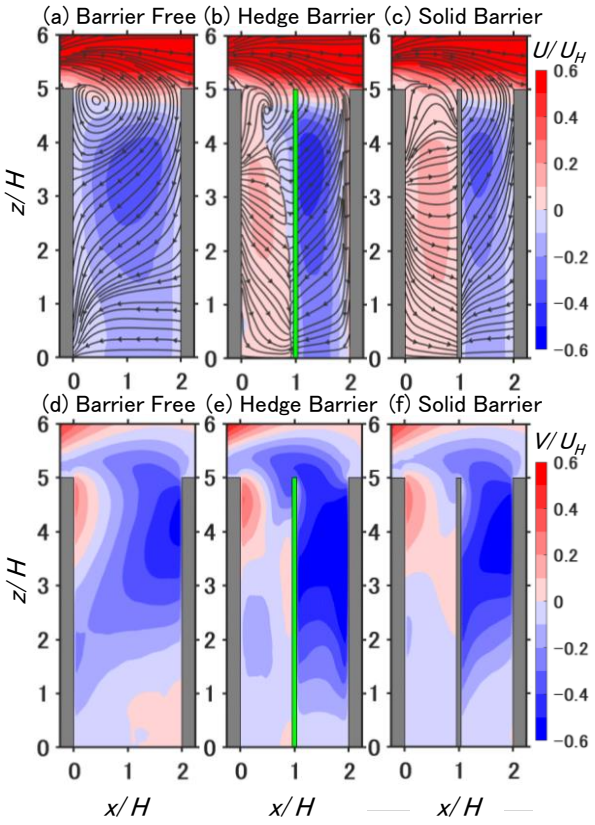


Fig. 8. Distributions of the time-averaged streamlines, streamwise velocity $U/U_H$ and spanwise velocity $V/U_H$ in the horizontal plane ($z/H$=0.08).

Fig. 8 shows the distributions of the time-averaged streamlines, streamwise velocity $U/U_H$ and spanwise velocity $V/U_H$ in the horizontal plane ($z/H$=0.08), which correspond to both the barrier height and the pedestrian height. For $U/U_H$, negative values were simulated in the barrier-free case because of the large recirculation flow shown in Fig. 7(a). In addition, a local recirculation zone was simulated near the intersection ($x/H$=0, $y/H$=5), which brought fresh air from the side of the canyon. Meanwhile, $U/U_H$ in hedge and solid barrier cases were generally in positive values between the leeward walls and the barriers, corresponding to the anticlockwise leeward vortices in Fig. 7(b) and (c). Further, the barriers weakened the recirculation zone near the intersection, especially in the solid barrier case. For $V/U_H$, hedge and solid barriers intensified the spanwise flow near the windward walls but weakened the spanwise flow near the leeward walls.

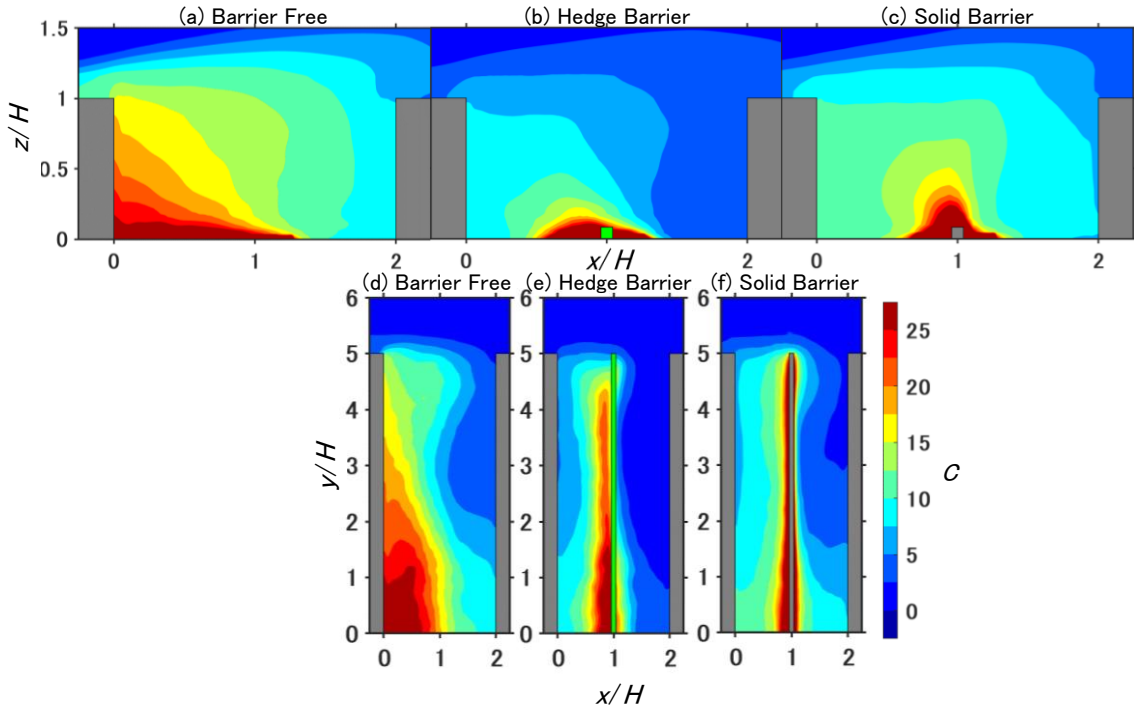


Fig. 9. Distributions of the time-averaged concentration $C$ in the (a-c) vertical plane ($y/H$=0) and (d-f) the horizontal plane ($z/H$=0.08).

Regarding the barrier effects on the concentration fields, Fig. 9 represents the distributions of the time-averaged concentration $C$ in the (a-c) vertical plane ($y/H$=0) and (d-f) the horizontal plane ($z/H$=0.08). In the barrier-free case, the pollutant was transported toward the leeward wall by the vertical recirculation flow and toward the inner part of the street by the spanwise flow, hence large values of $C$ can be found near the leeward wall. The pollutant in the barrier-free case was mainly removed from the street canyon near the top of the leeward wall as studied in Zhang et al. (2022) [46]. Hedge and solid barriers greatly influenced the $C$ distribution and significantly decreased $C$ in the street canyon (Table 2). Meanwhile, the two counter-direction vortices in the hedge and solid barrier cases transported the pollutant toward the center of the canyon ($x/H$=1), increasing the vertical pollutant removal at the top of the street canyon. Despite this decrease of the average concentration, large $C$ can be found along the barriers. Hence, in view of urban design issues, pollutant absorption methods [47] are expected to be combined with the barriers to achieve a better pollutant reduction effect. In addition, the solid barrier case generally showed larger values of $C$ than the hedge barrier case. The reason could be that the windward vortex, which was stronger in the hedge barrier case than that in the solid barrier case, dominated the pollutant removal.

Table 2 summarizes the spatially-averaged concentration in the barrier-free case and the

concentration ratio between the analysis cases and the barrier-free case near the leeward wall ($x/H$=0.06, -5≤$y/H$≤5, 0≤$z/H$≤1), windward wall ($x/H$=1.94, -5≤$y/H$≤5, 0≤$z/H$≤1) and the whole street canyon (0≤$x/H$≤2, -5≤$y/H$≤5, 0≤$z/H$≤1). The spatially-averaged concentration is the area-weighted average concentration on the planes. In the barrier-free case, the spatially-averaged concentration near the leeward wall was about 2.7 times the value near the windward wall and 1.5 times the canyon-averaged concentration. The hedge barrier reduced the spatially-averaged concentration by about 59% near the leeward wall, 64% near the windward wall and 45% for the whole street canyon compared to the barrier-free case. Although the pollutant reduction effect of the solid barrier was less than that of the hedge barrier, the solid barrier reduced spatially-averaged concentration by about 45% near the leeward wall, 20% near the windward wall and 17% for the whole street canyon.

Table 2. Spatially-averaged concentration ratio between the analysis and the barrier-free cases. The values are based on the leeward wall ($x/H$=0.06, -5≤$y/H$≤5, 0≤$z/H$≤1), windward wall ($x/H$=1.94, -5≤$y/H$≤5, 0≤$z/H$≤1) and street canyon (0≤$x/H$≤2, -5≤$y/H$≤5, 0≤$z/H$≤1). The values in parenthesis indicate the spatially-averaged concentration in the barrier-free case.

| Barrier type | Leeward | Windward | Canyon |
|---|---|---|---|
| Perpendicular wind direction | | | |
| Free | 100.0 (13.8) | 100.0 (5.0) | 100.0 (9.0) |
| Hedge (LAD=4.2 $m^2/m^3$, Width=1.5 m) | 41.1 | 36.4 | 54.5 |
| Hedge (LAD=2.0 $m^2/m^3$, Width=1.5 m) | 41.0 | 36.1 | 54.1 |
| Hedge (LAD=1.0 $m^2/m^3$, Width=1.5 m) | 43.1 | 36.6 | 53.2 |
| Hedge (LAD=4.2 $m^2/m^3$, Width=1.0 m) | 41.4 | 34.2 | 53.2 |
| Hedge (LAD=4.2 $m^2/m^3$, Width=0.5 m) | 41.8 | 35.0 | 51.8 |
| Solid (Width=1.5 m) | 55.2 | 80.7 | 83.3 |
| Solid (Width=1.0 m) | 57.2 | 80.0 | 86.8 |
| Solid (Width=0.5 m) | 59.8 | 83.1 | 87.2 |
| Oblique wind direction | | | |
| Free | 100.0 (2.5) | 100.0 (0.3) | 100.0 (1.3) |
| Hedge (LAD=4.2 $m^2/m^3$, Width=1.5 m) | 69.1 | 70.2 | 132.5 |
| Solid (Width=1.5 m) | 42.0 | 39.8 | 95.9 |

### 3.3 Concentration flux of basic cases

Convective concentration flux and turbulent concentration flux are crucial for understanding the pollutant transport in urban environments [48–50]. To clarify the effect of the hedge and solid barriers on pollutant removal in the street canyon, we investigated the surface-sum concentration flux, as shown in Table 3. $u'$, $v'$, $w'$ are the fluctuation velocities in the streamwise, spanwise and vertical directions, respectively. The pollutants were transported out of the street canyon from the vertical convective concentration flux $WC$ and vertical turbulent concentration flux $\overline{w'c'}$ at the

top plane ($0 \le x/H \le 2$, $-5 \le y/H \le 5$, $z/H=1$), and also from the spanwise convective concentration flux $VC$ and spanwise turbulent concentration flux $\overline{v'c'}$ at the side planes ($0 \le x/H \le 2$, $y/H=-5$ and $y/H=5$, $0 \le z/H \le 1$). The positive and negative values indicate the outflow and inflow concentration flux, respectively. The percentage value (ratio of each surface-sum concentration flux to the net concentration flux) was used to represent the contribution of each concentration flux. In addition, the difference of the net concentration flux between the barrier free, hedge barrier and solid barrier cases were confirmed smaller than 0.5 percent.

Table 3 Surface-sum concentration flux at the top plane ($0 \le x/H \le 2$, $-5 \le y/H \le 5$, $z/H=1$) and the side planes ($0 \le x/H \le 2$, $y/H=-5$ and $y/H=5$, $0 \le z/H \le 1$). The positive and negative values indicate the outflow and inflow concentration flux, respectively. All values are represented by percentages (ratio of each surface-sum concentration flux to net concentration flux). The values in parentheses are the nondimensionalized net concentration-flux.

| Concentration flux | Free | Hedge (LAD=4.2 $m^2/m^3$, Width=1.5 m) | Solid (Width=1.5 m) |
|---|---|---|---|
| $WC$ at the top plane | 81% | 65% | 75% |
| $\overline{w'c'}$ at the top plane | 25% | 41% | 32% |
| $VC$ at the side planes | -16% | -17% | -23% |
| $\overline{v'c'}$ at the side planes | 10% | 11% | 16% |
| Net concentration flux | 100% (1791) | 100% (1783) | 100% (1797) |

For the barrier free case, $WC$ and $\overline{w'c'}$ at the top plane primarily determined the removal process compared to $VC$ and $\overline{v'c'}$ at the side planes because the surface area of the top plane was larger than the side planes (Table 3). In addition, $WC$ dominated the removal process at the top plane compared to $\overline{w'c'}$ as shown in Fig. 10 (a, d). Large positive $WC$ occurred near the leeward wall and small negative $WC$ occurred near the windward wall. These results were in line with the findings in two-dimensional street canyons in the previous wind tunnel experiment [51] and LES studies [52]. For the side planes, although positive $VC$ occurred near the leeward wall, the surface-sum $VC$ was negative because the separate flow near the building edges (Fig. 8 (a)) leaded to large pollutant inflow to the street canyon. At the same time, $\overline{v'c'}$ was generally positive at the side planes, especially large positive $\overline{v'c'}$ occurred near the ground.

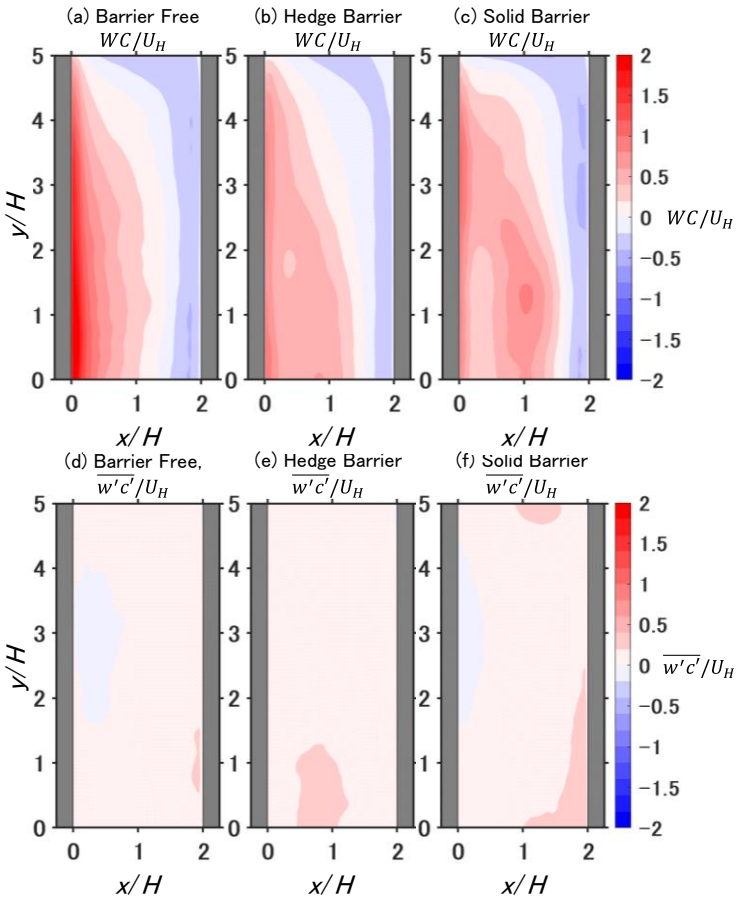


Fig. 10. Distributions of the vertical convective concentration flux $WC/U_H$ and vertical turbulent concentration flux $\overline{w'c'}/U_H$ in the top plane ($0 \leq x/H \leq 2$, $-5 \leq y/H \leq 5$, $z/H=1$) of the street canyon.

Previous LES studies found that the rooftop obstacles [52] and building façade geometrical details [53] increased $\overline{w'c'}$ at the top plane and enhanced the pollutant removal in the street canyon. Similarly, the hedge and solid barriers decreased surface-sum $WC$ and increased surface-sum $\overline{w'c'}$ at the top plane from the barrier free case as shown in Table 3. In addition, the hedge barrier case showed larger surface-sum $WC$ decrease and larger surface-sum $WC$ increase from the barrier free case than the solid barrier case. Due to the reshaped vertical vortices (
Fig. 7 (a-c)), the hedge and solid barrier cases showed smaller $WC$ near the leeward wall but larger $WC$ above the barriers compared to the barrier free case (Fig. 10). For the side planes, the hedge and solid barriers increased both inflow $VC$ and outflow $\overline{v'c'}$ from the barrier free case, especially near the barriers (Fig. 11).

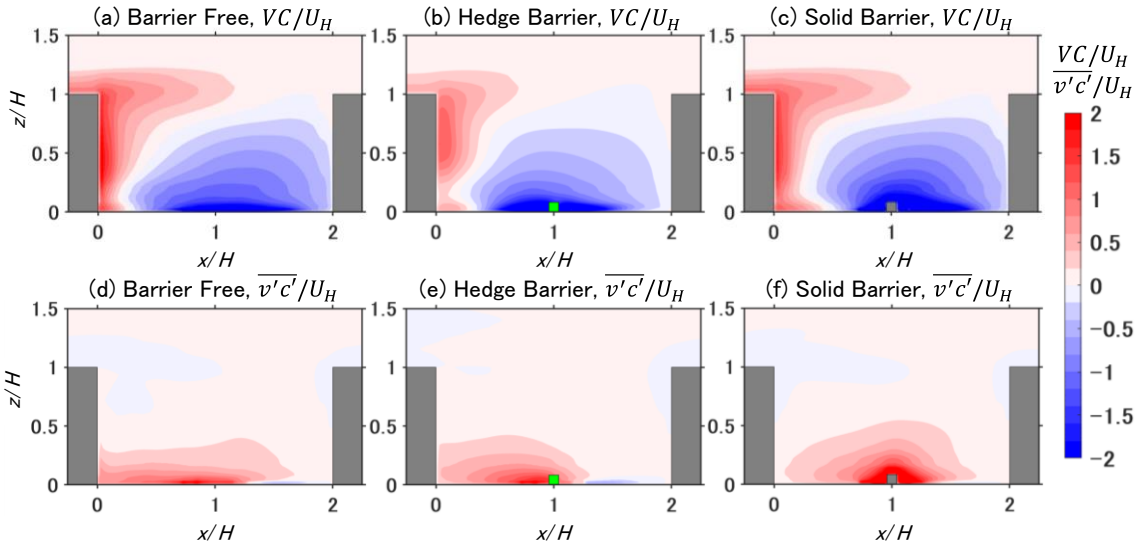


403

404 Fig. 11. Distributions of the spanwise convective concentration flux $VC/U_H$ and spanwise
405 turbulent concentration flux $\overline{v'c'}/U_H$ in the side plane ($0 \leq x/H \leq 2$, $y/H=5$, $0 \leq z/H \leq 1$) of the street
406 canyon.

407

### 3.4 Influence of leaf area density

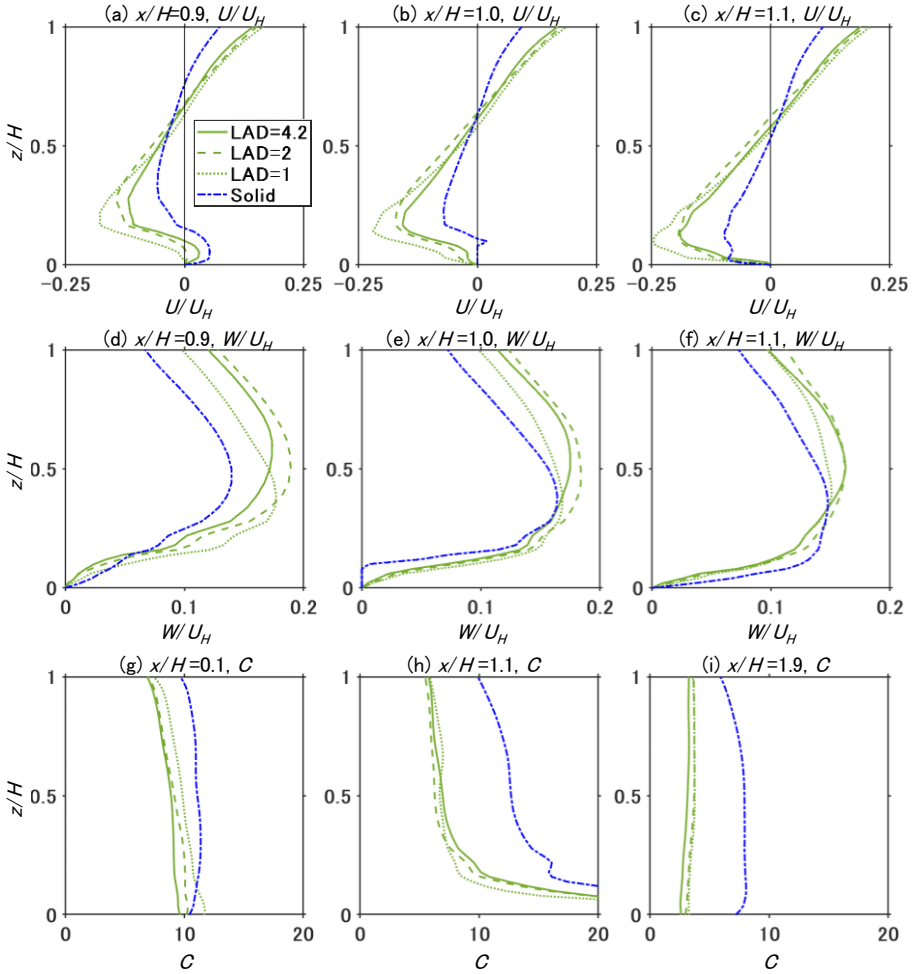


Fig. 12. Vertical profiles of the time-averaged streamwise velocity $U/U_H$, vertical velocity $W/U_H$, concentration $C$ in the vertical plane ($y/H$=0) with different LAD.

To understand the influence of the hedge LAD on the flow and concentration fields, Fig. 12 shows the vertical profiles of the time-averaged streamwise velocity $U/U_H$, vertical velocity $W/U_H$ and concentration $C$ in the vertical plane ($y/H$=0) for different LAD (1, 2 and 4.2 $m^2/m^3$). For comparison, the results based on the solid barrier are also shown. A decrease of LAD intensified the negative $U/U_H$ near the ground as shown in Fig. 12 (a-c). At the same time, a decrease of LAD also increased $W/U_H$ near the ground near the leeward side of the barrier (Fig. 12 (d)). These can be attributed to that small LAD resulted in less momentum reduction when recirculation flow passed through the hedge barriers, therefore resulted in large windward vortices and small leeward vortices as shown in

Fig. 7. In addition, the $U/U_H$ differences between LAD=4.2 $m^2/m^3$ and LAD=2 $m^2/m^3$ were smaller than the differences between LAD=2 $m^2/m^3$ and LAD=1 $m^2/m^3$.

For the time-averaged concentration $C$, decreasing the LAD led to lower values at the center of the street due to increased $U/U_H$ (Fig. 12 (h)). Meanwhile, the stronger negative $U/U_H$ transported more pollutant toward the leeward walls and therefore increased $C$ (Fig. 12 (g)). Regarding the spatially-averaged concentration (Table 2), the hedge barrier with LAD=1 $m^2/m^3$ showed slightly higher $C$ near the leeward wall and windward wall but smaller $C$ for the whole street canyon compared to the hedge barrier with LAD=4.2 $m^2/m^3$. Meanwhile, the hedge barrier with LAD=2 $m^2/m^3$ showed comparable $C$ to the hedge barrier with LAD=4.2 $m^2/m^3$. As the pollutant was emitted at the ground which was lower than the barrier height in the current study, the small wind velocity change near the hedge barriers due to the LAD change led to small effect on concentration.

### 3.5 Influence of barrier width

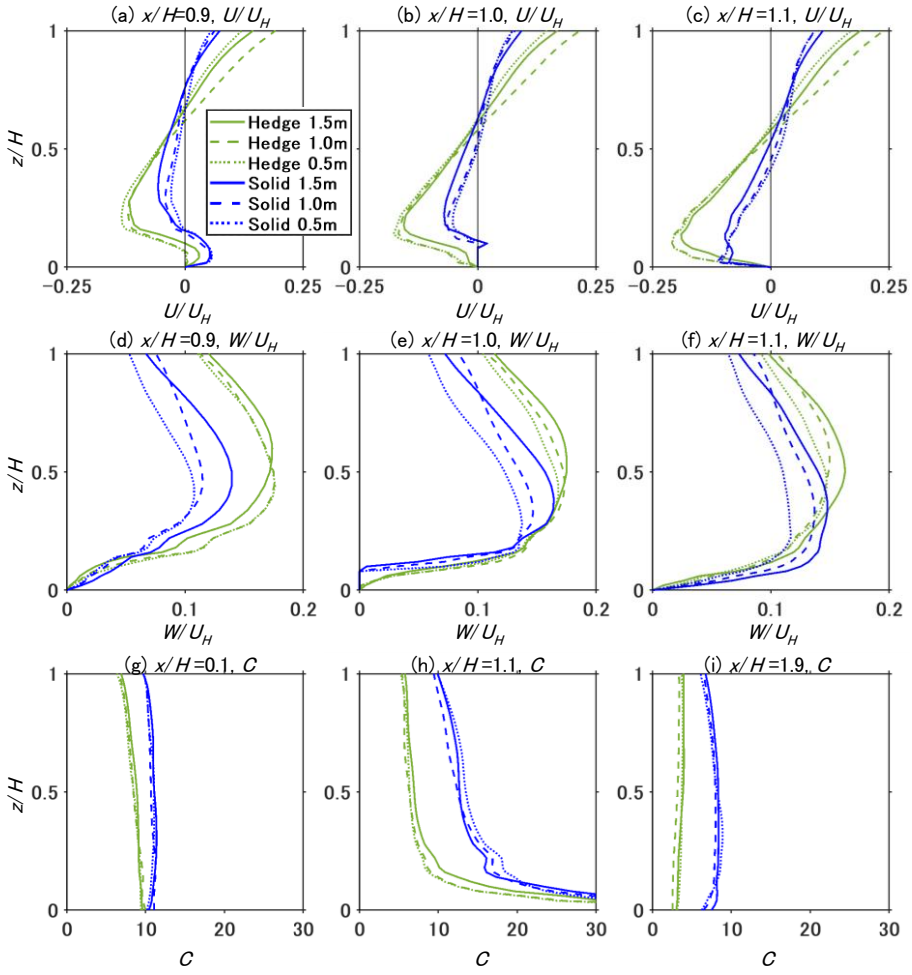


Fig. 13. Vertical profiles of the time-averaged streamwise velocity $U/U_H$, vertical velocity $W/U_H$, concentration $C$ in the vertical plane ($y/H$=0) with different barrier widths.

Regarding the influence of hedge and solid barrier width, Fig. 13 shows vertical profiles of time-averaged streamwise velocity $U/U_H$, vertical velocity $W/U_H$ and concentration $C$ in the vertical plane ($y/H$=0) with different barrier widths (0.5, 1.0 and 1.5 m). For hedge barriers, decreasing barrier width resulted in similar influences on the flow and concentration fields as decreasing LAD. Specifically, the negative $U/U_H$ near the ground was enhanced and $W/U_H$ near the leeward side of the barrier was increased. In addition, decreasing hedge barrier width increased the spatially-averaged concentration near the leeward and windward walls but decreased the spatially-averaged concentration in the street canyon as shown in Table 2.

However, decreasing solid barrier width generally weakened both $U/U_H$ and $W/U_H$ in the street, indicating that a thinner solid barrier led to a smaller change of the near-ground wind direction from horizontal to slanting upwards. As a result, decreasing solid barrier width hindered the pollutant removal at the top of the canyon and therefore increased the spatially averaged concentration (Table 2) in the street canyon.

In general, increasing hedge and solid barrier width did not show significant effects on the flow and concentration fields in the street canyon, indicating that the presence of a line obstacle on the street ground was the dominant reason for reducing the pollutant concentration by breaking the large recirculation flow (
Fig. 7).

### 3.6 Influence of oblique wind direction

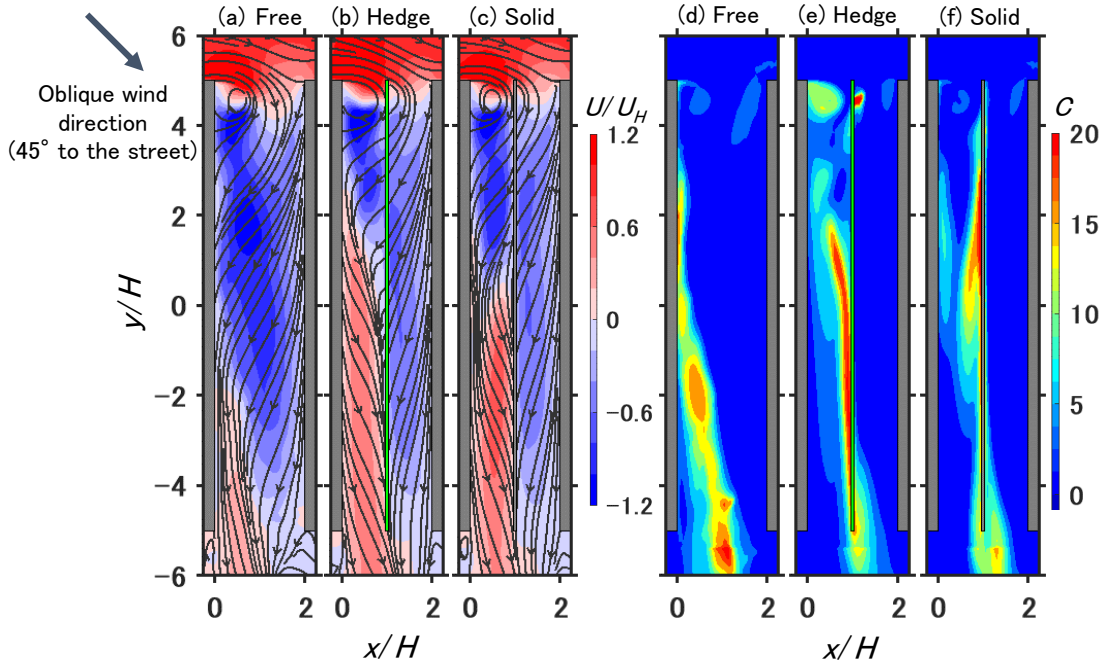


Fig. 14. Distributions of the time-averaged streamlines, streamwise streamlines, velocity $U/U_H$ and time-averaged concentration $C$ in the horizontal plane ($z/H$=0.08) under the oblique wind direction.

To discuss the influence of wind direction, simulations of the basic cases (barrier-free, hedge barrier with LAD=4.2 $m^2/m^3$ and solid barrier) were conducted under the oblique wind direction, which was 45 degrees to the street. Fig. 14 shows the distributions of the time-averaged streamlines, streamwise velocity $U/U_H$ and time-averaged concentration $C$ in the horizontal plane ($z/H$=0.08). In the barrier-free case, the oblique wind direction resulted in a large region with negative $U/U_H$ in the street canyon (Fig. 14 (a)), therefore the pollutant was concentrated near the leeward wall (Fig. 14 (d)). In addition, the air exchange in the canyon increased in the street canyon in the oblique wind direction compared to the perpendicular wind direction. Therefore, the spatially-averaged concentration near the leeward wall, the windward wall and in the whole street canyon reduced to 18%, 6%, and 14% of values in the barrier-free case in the perpendicular wind direction, respectively (Table 2).

In the hedge and solid barrier cases, positive $U/U_H$ regions were observed between the leeward walls and the barriers (Fig. 14 (b, c)), indicating that the barriers broke the recirculation flows into the leeward and windward vortices, similarly to the perpendicular wind directions (Fig. 8). Therefore, the leeward and windward vortices carried the pollutant along the leeward sides of the hedge and solid barriers (Fig. 14 (e, f)). Meanwhile, the permeability of the barriers resulted in

different streamlines near $y/H$=2 and therefore leaded to different locations of the high-concentration area in the hedge and solid barrier cases. The hedge barrier led to higher $C$ than the solid barrier at the corner of the canyon and on the leeward side of the barrier. Regarding the spatially-averaged concentration, compared to the barrier-free case (Table 2), the hedge barrier reduced it by about 30% at both the leeward and windward walls, but increased it by 30% in average over the whole street canyon due to the high concentration areas along the barrier. However, the solid barrier reduced it by about 60% at both leeward and windward walls compared to the barrier-free case, and by 4% in average over the whole street canyon. Therefore, both hedge and solid barriers were effective in reducing pollutant concentrations near the building walls in an oblique wind direction, and the solid barrier showed better effects than the hedge barrier.

## 4 Conclusions

### 4.1 Summary

Road barriers have been considered as effective methods to mitigate traffic pollution in urban environments. Meanwhile, the effect of road barriers on the flow and concentration fields in streets has not been sufficiently studied. To address this knowledge gap, this study conducted large-eddy simulations on pollutant reduction effect of hedge and solid barriers in an idealized street canyon. The aspect ratio of the street canyon was 0.5 and the building height was 18 m. The 1.5 m high barriers were placed in the middle of the street. The pollutant was emitted from the line sources at ground level. After validating the LES results with wind tunnel experiments, the influences of LAD and barrier width were investigated. Furthermore, the barrier effects were also studied in an oblique wind direction. The major findings are summarized below:

(1) LES accurately reproduced the concentration distributions for both the leeward and windward sides in the barrier-free case. In addition, LES well reproduced the barrier-induced pollutant reduction. Therefore, LES was considered to be an effective method for analyzing the barrier effect.

(2) For the flow fields in the street canyon, a large recirculation vortex was observed in the barrier-free case. However, the road center barriers modified the recirculated air flow with additional vortices between the leeward walls and the barriers. In addition, the hedge barrier case showed a stronger windward vortex compared to the solid barrier case because the recirculated airflow could pass through the permeable hedge barrier but was forced over the solid barrier. At the same time, a stronger leeward vortex was formed in the solid barrier case than in the hedge barrier case.

(3) For the concentration field in the barrier-free case, the pollutant was transported toward the leeward wall by the vertical recirculation flow and toward the inner part of the street by the spanwise flow, hence large concentration regions were found near the leeward wall. However, the two counter-direction vortices in the hedge and solid barrier cases transported the pollutant toward the center of the canyon and enhanced the vertical pollutant removal at the top of the street canyon. The hedge barrier reduced the spatially-averaged concentration by about 59% near the leeward wall, 64% near the windward wall and 45% over the whole street canyon. The solid barrier was less effective: it reduced the spatially-averaged concentration by about 45% near the leeward wall, 20% near the windward wall, and 17% over the whole street canyon.

(4) Decreasing the hedge LAD resulted in less momentum reduction when recirculation flow passed through the hedge barriers, therefore intensified the streamwise and vertical velocity in the street. The increased streamwise wind transported more efficiently the pollutant toward the leeward walls and therefore increased concentration near the leeward wall. Meanwhile, the increased vertical wind enhanced pollutant removal at the top of the canyon and therefore decreased canyon-averaged concentration. In addition, the differences between LAD=4.2 $m^2/m^3$ and LAD=2 $m^2/m^3$ were smaller than the differences between LAD=2 $m^2/m^3$ and LAD=1 $m^2/m^3$. One of the reasons was considered to be that the wind velocity near the barriers was small, and therefore further increasing the LAD led to little effect on velocity reduction.

(5) Decreasing hedge barrier width resulted in similar effects on the flow and concentration fields as decreasing LAD. However, decreasing the solid barrier width generally weakened the wind velocity in the street. This is because thinner solid barriers led to smaller influences to change the near-ground wind direction from horizontal to slanting upwards. As a result, decreasing solid barrier width hindered the pollutant removal at the top of the canyon and therefore increased the spatially-averaged concentration in the street canyon. In general, varying barrier width from 0.5 m to 1.5 m did not show significant effects on the flow and concentration fields in the street canyon because the presence of a line obstacle on the street ground was the dominant reason for reducing the pollutant concentration by breaking the large recirculation flow.

(6) In an oblique wind direction of 45 degrees to the street, the pollutant was concentrated on the leeward side in the street canyon in the barrier-free case. In the hedge and solid barrier cases, the barriers broke the recirculation flows into the leeward and windward vortices, similarly

to the perpendicular wind directions. The hedge and solid barriers reduced the spatially-averaged concentration near the building walls by almost 30% and 60% compared to the barrier-free case, respectively. Meanwhile, due to the high concentration regions along the barrier, the hedge barrier increased by 30% the spatially-averaged concentration in the street canyon and the solid barrier reduced it by about 4% compared to the barrier-free case.

In conclusion, the pollutant reduction effects of hedge and solid barriers were confirmed in both perpendicular and oblique wind directions. Although the effects of the variation in the hedge LAD and barrier width were not significant on the flow and concentration fields in the street canyon, increasing the hedge LAD and barrier width is recommended to reduce more efficiently pollutant concentrations near building walls. In addition, the hedge barrier is recommended in a perpendicular wind direction to the street, and the solid barrier is recommended in an oblique wind direction. The conclusions obtained in this study may help urban planners to design the location and material of barriers.

### 4.2 Limitations of the study

Although this study highlighted several key aspects, some limitations should be addressed in future work.

(1) Concerning the street configuration, barrier dimension and meteorological conditions, the isolated street canyon employed in the current study was a generic idealized urban geometry. Further studies are needed to evaluate the barrier effect in the real-world flow environment. For instance, traffic-induced turbulence could significantly change the impact of the barrier. In addition, although this study found that the barriers with a height of 1.5 and a width from 0.5 m to 1.5 m showed small differences in pollutant reduction effect, further studies are needed to confirm the pollutant reduction effect from larger barriers. Moreover, the isothermal boundary layer was considered, whereas solar radiation can lead to large temperature differences in the street and result in buoyant flows. Therefore, the barrier effects should be evaluated under different thermal conditions [54].

(2) Except of the hedge and solid barriers investigated in this study, other geometrical details in the street canyon such as wind catchers [55], car parking systems [56] and elevated walkways [57] can also influence the flow fields in the street and insert similar pollutant reduction mechanisms to the barriers. Their urban area applicability, efficacy and limitations were discussed in the literature review [6,7]. Therefore, it is of great importance to compare the effects of these geometric details in order to provide urban planners with appropriate

recommendations for reducing pollutant concentrations. However, these geometrical details have been evaluated in different street configurations and meteorological conditions such as wind direction, which makes the comprehensive comparisons difficult. Therefore, further studies are needed to set the same situations under the representative urban environments to evaluate these geometrical details.

(3) Regarding the hedge modeling, the dry deposition effect was not considered in the current study in accordance with the experiment. However, the deposition effect is dependent on the pollutant species [45], particle size and density [44] and LAD [17] and may provide a more comprehensive assessment of the hedge barrier volume and LAD.

(4) Chemical reactions and aerosol dynamics were not considered during the pollutant dispersion in the current study, whereas they have been found to significantly influence the distribution of traffic pollutants in the street canyon [58,59] and they should be considered to simulate the air quality more accurately.

## Declaration of competing interest

The authors declare that they have no known competing financial interests or personal relationships that could have appeared to influence the work reported in this paper.

## Acknowledgements

This work was partially funded by Ecole des Ponts ParisTech (Erasmus+ program). Yang Zhang's time for this work is supported by the Northeastern University Impact Engines program.

## Author contributions

Chao Lin: Methodology, Validation, Formal analysis, Investigation, Writing - Original Draft, Writing - Review & Editing, Visualization

Ryozo Ooka: Conceptualization, Resources, Supervision, Project administration, Formal analysis, Writing - Review & Editing

Hideki Kikumoto: Methodology, Resources, Supervision, Formal analysis, Writing - Review & Editing

Cédric Flageul: Formal analysis, Writing - Review & Editing

Youngseob Kim: Formal analysis, Writing - Review & Editing

Yunyi Wang: Formal analysis, Writing - Review & Editing

Alice Maison: Formal analysis, Writing - Review & Editing

Yang Zhang: Formal analysis, Writing - Review & Editing

Karine Sartelet: Conceptualization, Resources, Supervision, Formal analysis, Writing - Review & Editing

Reference


[1] P. Kumar, M. Khare, R.M. Harrison, W.J. Bloss, A.C. Lewis, H. Coe, L. Morawska, New directions: Air pollution challenges for developing megacities like Delhi, Atmos. Environ. 122 (2015) 657–661. doi:10.1016/j.atmosenv.2015.10.032.

[2] W.J. Guan, X.Y. Zheng, K.F. Chung, N.S. Zhong, Impact of air pollution on the burden of chronic respiratory diseases in China: time for urgent action, Lancet. 388 (2016) 1939–1951. doi:10.1016/S0140-6736(16)31597-5.

[3] P. Kumar, S. Jain, B.R. Gurjar, P. Sharma, M. Khare, L. Morawska, R. Britter, New Directions: Can a "blue sky" return to Indian megacities?, Atmos. Environ. 71 (2013) 198–201. doi:10.1016/J.ATMOSENV.2013.01.055.

[4] A. McNabola, N. O'Luanaigh, J. Gallagher, L. Gill, The development and assessment of an aspiration efficiency reducing system of air pollution control for particulate matter in building ventilation systems, Energy Build. 61 (2013) 177–184. doi:10.1016/j.enbuild.2013.02.024.

[5] J. Gallagher, R. Baldauf, C.H. Fuller, P. Kumar, L.W. Gill, A. McNabola, Passive methods for improving air quality in the built environment: A review of porous and solid barriers, Atmos. Environ. 120 (2015) 61–70. doi:10.1016/j.atmosenv.2015.08.075.

[6] Z. Li, T. Ming, T. Shi, H. Zhang, C.-Y. Wen, X. Lu, X. Dong, Y. Wu, R. de Richter, W. Li, C. Peng, Review on pollutant dispersion in urban areas-part B: Local mitigation strategies, optimization framework, and evaluation theory, Build. Environ. 198 (2021) 107890. doi:10.1016/j.buildenv.2021.107890.

[7] R. Buccolieri, O.S. Carlo, E. Rivas, J.L. Santiago, P. Salizzoni, M.S. Siddiqui, Obstacles influence on existing urban canyon ventilation and air pollutant concentration: A review of potential measures, Build. Environ. 214 (2022) 108905. doi:10.1016/j.buildenv.2022.108905.

[8] A. McNabola, New Directions: Passive control of personal air pollution exposure from traffic emissions in urban street canyons, Atmos. Environ. 44 (2010) 2940–2941. doi:10.1016/j.atmosenv.2010.04.005.

[9] R. Baldauf, Roadside vegetation design characteristics that can improve local, near-road air quality, Transp. Res. Part D Transp. Environ. 52 (2017) 354–361. doi:10.1016/j.trd.2017.03.013.

[10] A. McNabola, B.M. Broderick, L.W. Gill, A numerical investigation of the impact of low boundary walls on pedestrian exposure to air pollutants in urban street canyons, Sci. Total

664 Environ. 407 (2009) 760–769. doi:10.1016/j.scitotenv.2008.09.036.
665 [11] G.E. Bowker, R. Baldauf, V. Isakov, A. Khlystov, W. Petersen, The effects of roadside
666 structures on the transport and dispersion of ultrafine particles from highways, Atmos.
667 Environ. 41 (2007) 8128–8139. doi:10.1016/j.atmosenv.2007.06.064.
668 [12] D. Finn, K.L. Clawson, R.G. Carter, J.D. Rich, R.M. Eckman, S.G. Perry, V. Isakov, D.K.
669 Heist, Tracer studies to characterize the effects of roadside noise barriers on near-road
670 pollutant dispersion under varying atmospheric stability conditions, Atmos. Environ. 44
671 (2010) 204–214. doi:10.1016/j.atmosenv.2009.10.012.
672 [13] J. Gallagher, L.W. Gill, A. McNabola, Numerical modelling of the passive control of air
673 pollution in asymmetrical urban street canyons using refined mesh discretization schemes,
674 Build. Environ. 56 (2012) 232–240. doi:10.1016/j.buildenv.2012.03.013.
675 [14] C. Gromke, N. Jamarkattel, B. Ruck, Influence of roadside hedgerows on air quality in
676 urban street canyons, Atmos. Environ. 139 (2016) 75–86.
677 doi:10.1016/j.atmosenv.2016.05.014.
678 [15] A. Issakhov, A. Tursynzhanova, A. Abylkassymova, Numerical study of air pollution
679 exposure in idealized urban street canyons: Porous and solid barriers, Urban Clim. 43
680 (2022) 101112. doi:10.1016/j.uclim.2022.101112.
681 [16] Z. Tong, R.W. Baldauf, V. Isakov, P. Deshmukh, K. Max Zhang, Roadside vegetation
682 barrier designs to mitigate near-road air pollution impacts, Sci. Total Environ. 541 (2016)
683 920–927. doi:10.1016/j.scitotenv.2015.09.067.
684 [17] F. Xue, X. Li, The impact of roadside trees on traffic released PM10 in urban street
685 canyon: Aerodynamic and deposition effects, Sustain. Cities Soc. 30 (2017) 195–204.
686 doi:10.1016/j.scs.2017.02.001.
687 [18] A. Maison, C. Flageul, B. Carissimo, Y. Wang, A. Tuzet, K. Sartelet, Parameterizing the
688 aerodynamic effect of trees in street canyons for the street network model MUNICH using
689 the CFD model Code_Saturne, Atmos. Chem. Phys. 22 (2022) 9369–9388.
690 doi:10.5194/ACP-22-9369-2022.
691 [19] R. Buccolieri, J.-L. Santiago, E. Rivas, B. Sanchez, Review on urban tree modelling in
692 CFD simulations: Aerodynamic, deposition and thermal effects, Urban For. Urban Green.
693 31 (2018) 212–220. doi:10.1016/j.ufug.2018.03.003.
694 [20] M. Ghasemian, S. Amini, M. Princevac, The influence of roadside solid and vegetation
695 barriers on near-road air quality, Atmos. Environ. 170 (2017) 108–117.
696 doi:10.1016/j.atmosenv.2017.09.028.
697 [21] H.L. Brantley, G.S.W. Hagler, P. J. Deshmukh, R.W. Baldauf, Field assessment of the
698 effects of roadside vegetation on near-road black carbon and particulate matter, Sci. Total
699 Environ. 468–469 (2014) 120–129. doi:10.1016/J.SCITOTENV.2013.08.001.

[22] K.V. Abhijith, P. Kumar, Field investigations for evaluating green infrastructure effects on air quality in open-road conditions, Atmos. Environ. 201 (2019) 132–147. doi:10.1016/j.atmosenv.2018.12.036.

[23] T.B. Ottosen, P. Kumar, The influence of the vegetation cycle on the mitigation of air pollution by a deciduous roadside hedge, Sustain. Cities Soc. 53 (2020) 101919. doi:10.1016/J.SCS.2019.101919.

[24] P. Kumar, J.C. Zavala-Reyes, M. Tomson, G. Kalaiarasan, Understanding the effects of roadside hedges on the horizontal and vertical distributions of air pollutants in street canyons, Environ. Int. 158 (2022) 106883. doi:10.1016/j.envint.2021.106883.

[25] Y. Tominaga, T. Stathopoulos, CFD modeling of pollution dispersion in a street canyon: Comparison between LES and RANS, J. Wind Eng. Ind. Aerodyn. 99 (2011) 340–348. doi:10.1016/j.jweia.2010.12.005.

[26] C. Lin, R. Ooka, H. Kikumoto, T. Sato, M. Arai, CFD simulations on high-buoyancy gas dispersion in the wake of an isolated cubic building using steady RANS model and LES, Build. Environ. 188 (2021) 107478. doi:10.1016/j.buildenv.2020.107478.

[27] C. Gromke, B. Ruck, Pollutant Concentrations in Street Canyons of Different Aspect Ratio with Avenues of Trees for Various Wind Directions, Boundary-Layer Meteorol. 144 (2012) 41–64. doi:10.1007/s10546-012-9703-z.

[28] Y. Tominaga, A. Mochida, R. Yoshie, H. Kataoka, T. Nozu, M. Yoshikawa, T. Shirasawa, AIJ guidelines for practical applications of CFD to pedestrian wind environment around buildings, J. Wind Eng. Ind. Aerodyn. 96 (2008) 1749–1761. doi:10.1016/j.jweia.2008.02.058.

[29] S.M. Salim, R. Buccolieri, A. Chan, S. Di Sabatino, Numerical simulation of atmospheric pollutant dispersion in an urban street canyon: Comparison between RANS and LES, J. Wind Eng. Ind. Aerodyn. 99 (2011) 103–113. doi:10.1016/j.jweia.2010.12.002.

[30] W. Li, Y. He, Y. Zhang, J. Su, C. Chen, C.W. Yu, R. Zhang, Z. Gu, LES simulation of flow field and pollutant dispersion in a street canyon under time-varying inflows with TimeVarying-SIMPLE approach, Build. Environ. 157 (2019) 185–196. doi:10.1016/j.buildenv.2019.04.049.

[31] OpenFOAM, OpenFOAM user guide, (2020). https://www.openfoam.com/.

[32] F. Nicoud, F. Ducros, Subgrid-scale stress modelling based on the square of the velocity gradient tensor, Flow, Turbul. Combust. 62 (1999) 183–200. doi:10.1023/A:1009995426001.

[33] J. Liu, J. Niu, Y. Du, C.M. Mak, Y. Zhang, LES for pedestrian level wind around an idealized building array—Assessment of sensitivity to influencing parameters, Sustain. Cities Soc. 44 (2019) 406–415. doi:10.1016/j.scs.2018.10.034.

[34] J. Burman, L. Jonsson, A. Rutgersson, On possibilities to estimate local concentration variations with CFD-LES in real urban environments, Environ. Fluid Mech. 19 (2019) 719–750. doi:10.1007/s10652-018-9650-4.

[35] A. Harten, On a Class of High Resolution Total-Variation-Stable Finite-Difference Schemes, SIAM J. Numer. Anal. 21 (1984) 1–23. doi:10.1137/0721001.

[36] H.C. Yee, Construction of explicit and implicit symmetric TVD schemes and their applications, J. Comput. Phys. 68 (1987) 151–179. doi:10.1016/0021-9991(87)90049-0.

[37] M. Antonopoulos-Domis, Large-eddy simulation of a passive scalar in isotropic turbulence, J. Fluid Mech. 104 (1981) 55–79. doi:10.1017/S0022112081002814.

[38] M. Klein, A. Sadiki, J. Janicka, A digital filter based generation of inflow data for spatially developing direct numerical or large eddy simulations, J. Comput. Phys. 186 (2003) 652–665. doi:10.1016/S0021-9991(03)00090-1.

[39] KIT, CODASC data base, Laboratory of Building & Environmental Aerodynamics. Karlsruhe Institute of Technology, (2017). http://www.windforschung.de/CODASC.htm.

[40] D.B. Spalding, A Single Formula for the "Law of the Wall," J. Appl. Mech. 28 (1961) 455–458. doi:10.1115/1.3641728.

[41] W.A. McMullan, M. Angelino, The effect of tree planting on traffic pollutant dispersion in an urban street canyon using large eddy simulation with a recycling and rescaling inflow generation method, J. Wind Eng. Ind. Aerodyn. 221 (2022) 104877. doi:10.1016/j.jweia.2021.104877.

[42] R. Buccolieri, J.-L. Santiago, E. Rivas, B. Sáanchez, Reprint of: Review on urban tree modelling in CFD simulations: Aerodynamic, deposition and thermal effects, Urban For. Urban Green. 37 (2019) 56–64. doi:10.1016/j.ufug.2018.07.004.

[43] X. Zhu, X. Wang, L. Lei, Y. Zhao, The influence of roadside green belts and street canyon aspect ratios on air pollution dispersion and personal exposure, Urban Clim. 44 (2022) 101236. doi:10.1016/j.uclim.2022.101236.

[44] L. Zhang, S. Gong, J. Padro, L. Barrie, A size-segregated particle dry deposition scheme for an atmospheric aerosol module, Atmos. Environ. 35 (2001) 549–560. doi:10.1016/S1352-2310(00)00326-5.

[45] L. Zhang, J.R. Brook, R. Vet, A revised parameterization for gaseous dry deposition in air-quality models, Atmos. Chem. Phys. 3 (2003) 2067–2082. doi:10.5194/acp-3-2067-2003.

[46] B. Zhang, R. Ooka, H. Kikumoto, Spatiotemporal Spectral Analysis of Turbulent Structures and Pollutant Removal in Two-Dimensional Street Canyon, Boundary-Layer Meteorol. 185 (2022) 63–91. doi:10.1007/s10546-022-00724-7.

[47] E. Brattich, F. Barbano, B. Pulvirenti, F. Pilla, M. Bacchetti, S. Di Sabatino, The effect of

772 photocatalytic coatings on NOx concentrations in real-world street canyons, Build.
773 Environ. 205 (2021). doi:10.1016/j.buildenv.2021.108312.
774 [48] P. Gousseau, B. Blocken, G.J.F. van Heijst, CFD simulation of pollutant dispersion around
775 isolated buildings: On the role of convective and turbulent mass fluxes in the prediction
776 accuracy, J. Hazard. Mater. 194 (2011) 422–434. doi:10.1016/j.jhazmat.2011.08.008.
777 [49] Y. Tominaga, T. Stathopoulos, CFD Modeling of Pollution Dispersion in Building Array:
778 Evaluation of turbulent scalar flux modeling in RANS model using LES results, J. Wind
779 Eng. Ind. Aerodyn. 104–106 (2012) 484–491. doi:10.1016/j.jweia.2012.02.004.
780 [50] A. Di Bernardino, P. Monti, G. Leuzzi, G. Querzoli, Pollutant fluxes in two-dimensional
781 street canyons, Urban Clim. 24 (2018) 80–93. doi:10.1016/j.uclim.2018.02.002.
782 [51] D. Marucci, M. Carpentieri, Effect of local and upwind stratification on flow and
783 dispersion inside and above a bi-dimensional street canyon, Build. Environ. 156 (2019)
784 74–88. doi:10.1016/j.buildenv.2019.04.013.
785 [52] C. Cintolesi, B. Pulvirenti, S. Di Sabatino, Large-Eddy Simulations of Pollutant Removal
786 Enhancement from Urban Canyons, Boundary-Layer Meteorol. 180 (2021) 79–104.
787 doi:10.1007/s10546-021-00610-8.
788 [53] X. Zheng, H. Montazeri, B. Blocken, Impact of building façade geometrical details on
789 pollutant dispersion in street canyons, Build. Environ. 212 (2022).
790 doi:10.1016/J.BUILDENV.2021.108746.
791 [54] Y. Zhao, L.W. Chew, A. Kubilay, J. Carmeliet, Isothermal and non-isothermal flow in
792 street canyons: A review from theoretical, experimental and numerical perspectives, Build.
793 Environ. 184 (2020) 107163. doi:10.1016/j.buildenv.2020.107163.
794 [55] K. Zhang, G. Chen, Y. Zhang, S. Liu, X. Wang, B. Wang, J. Hang, Integrated impacts of
795 turbulent mixing and NOX-O3 photochemistry on reactive pollutant dispersion and intake
796 fraction in shallow and deep street canyons, Sci. Total Environ. 712 (2020) 135553.
797 doi:10.1016/j.scitotenv.2019.135553.
798 [56] J. Gallagher, C. Lago, How parked cars affect pollutant dispersion at street level in an
799 urban street canyon? A CFD modelling exercise assessing geometrical detailing and
800 pollutant decay rates, Sci. Total Environ. 651 (2019) 2410–2418.
801 doi:10.1016/j.scitotenv.2018.10.135.
802 [57] L. Chen, C.M. Mak, J. Hang, Y. Dai, J. Niu, K.T. Tse, Large eddy simulation study on
803 pedestrian-level wind environments around elevated walkways and influential factors in
804 ideal urban street canyons, Build. Environ. 235 (2023) 110236.
805 doi:10.1016/j.buildenv.2023.110236.
806 [58] C. Lin, Y. Wang, R. Ooka, C. Flageul, Y. Kim, H. Kikumoto, Z. Wang, K. Sartelet,
807 Modeling of street-scale pollutant dispersion by coupled simulation of chemical reaction,

aerosol dynamics, and CFD, Atmos. Chem. Phys. 23 (2023) 1421–1436. doi:10.5194/acp-23-1421-2023.

[59] Y. Wang, C. Flageul, A. Maison, B. Carissimo, K. Sartelet, Impact of trees on gas concentrations and condensables in a 2-D street canyon using CFD coupled to chemistry modeling, Environ. Pollut. 323 (2023) 121210. doi:10.1016/j.envpol.2023.121210.

## Appendix A. Analysis on grid resolution independence

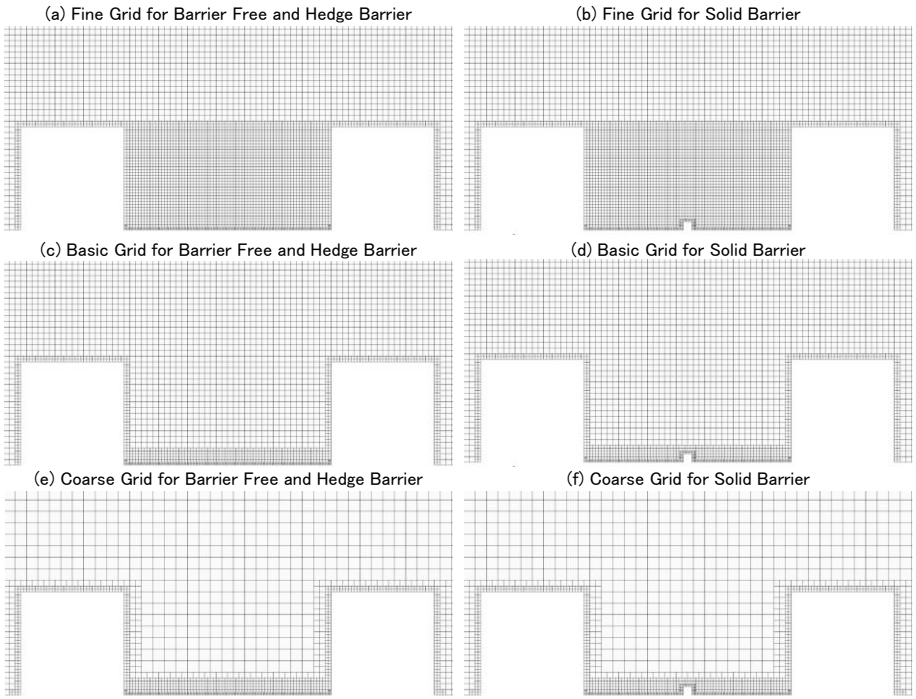


Fig. A1. Tested grid resolutions in the street canyon.

Grid sensitivity analysis was performed using coarse ($1.2 \times 10^6$), basic ($1.5 \times 10^6$), and fine ($1.8 \times 10^6$) grids as shown in Fig. A1. The smallest grid lengths near the source were $H/72$ in all grid resolutions. The largest grid lengths in the street canyon were $H/9$, $H/18$ and $H/36$ in the coarse, basic and fine resolutions, respectively.

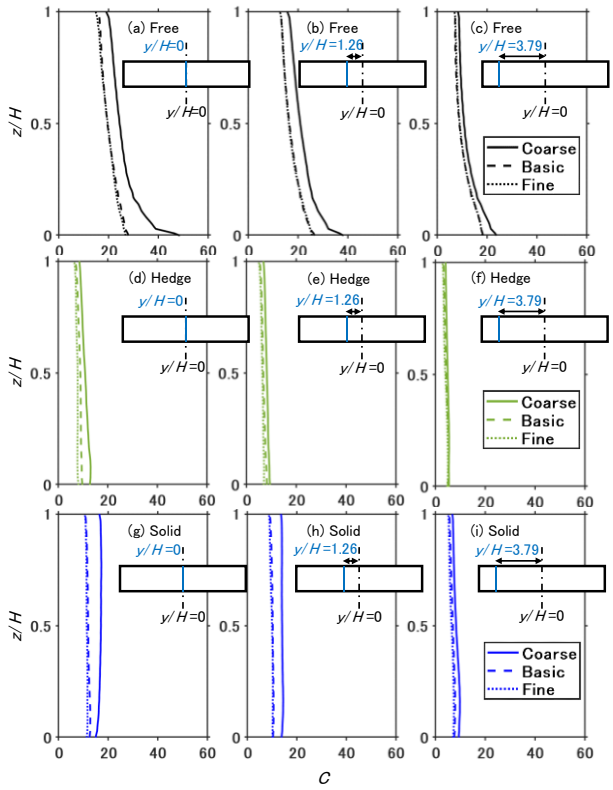


Fig. A2. Vertical profiles of the time-averaged concentration $C$ near the leeward wall ($x/H$=0.06) with different grid resolutions. The wind direction was perpendicular to the street.

Fig. A2 compares the vertical profiles of the time-averaged concentration $C$ near the leeward wall ($x$/H=0.06) with different grid resolutions for the barrier-free, hedge barrier and solid barrier cases. No significant discrepancy was observed between the results based on the basic and fine grids. However, the predicted mean concentration based on the coarse grid showed larger values compared to the other grid resolutions.

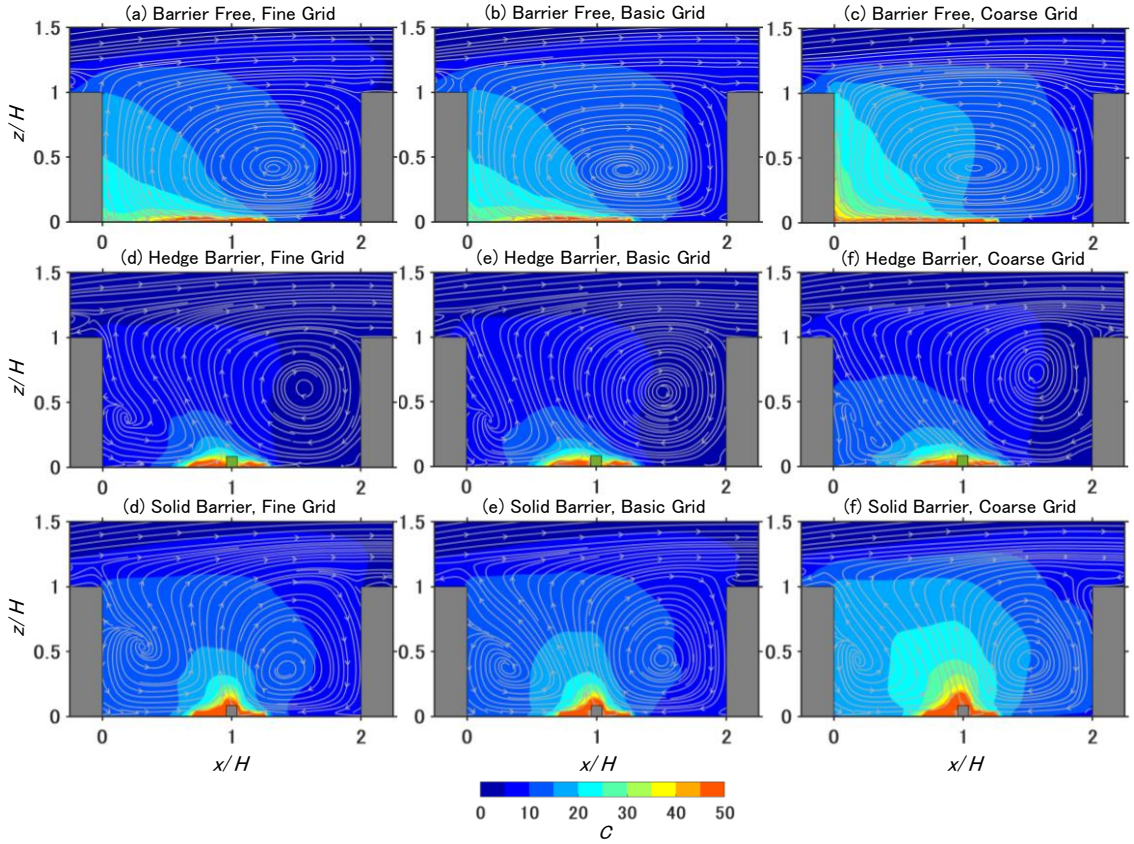


831

832 Fig. A3. Distributions of the time-averaged streamlines and concentration $C$ in the vertical plane
833 ($y/H$=0) with different grid resolutions. The wind direction was perpendicular to the street.

834

835 Furthermore, Fig. A3 compares the distributions of time-averaged streamlines and concentration
836 $C$ in the vertical plane ($y/H$=0) with different grid resolutions. For the barrier-free cases, no
837 significant discrepancy was observed between the streamlines based on different grid resolutions.
838 For the hedge barrier cases, the vortex center of the windward vortex based on the coarse grid
839 was higher than those based on the other grid resolutions. For the solid barrier cases, although
840 small discrepancies were observed between the vortex centers of the leeward vortices based on
841 different grid resolutions, the time-averaged concentration based on the basic grid and the fine
842 grid were close and larger than those based on the coarse grid.

843

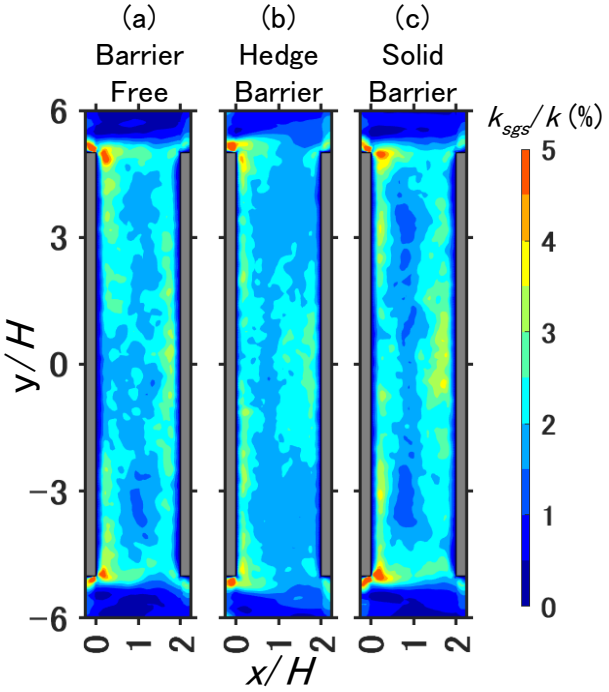


Fig. A4. Distributions of the ratio of the time-averaged turbulent kinetic energy at the subgrid scale $k_{sgs}$ and the time-averaged turbulent kinetic energy $k$ at the resolved scale and the in the horizontal plane ($z/H$=0.5) based on the basic grid. The wind direction was perpendicular (90 degrees) to the street.

In addition, Fig. A4 shows the distributions of the ratio of the time-averaged turbulent kinetic energy at the subgrid scale $k_{sgs}$ and the time-averaged turbulent kinetic energy $k$ at the resolved scale and the in the horizontal plane ($z/H$=0.5) based on the basic grid. The turbulent kinetic energy at the subgrid scale was calculated based on the WALE model [32] and was time-averaged during the sampling duration. Over 95% of the time-averaged turbulent kinetic energy was resolved by the LES using the basic grid. Therefore, the basic grid was adopted for the following simulations.

## Appendix B. Horizontal distributions of simulation results in the street canyon

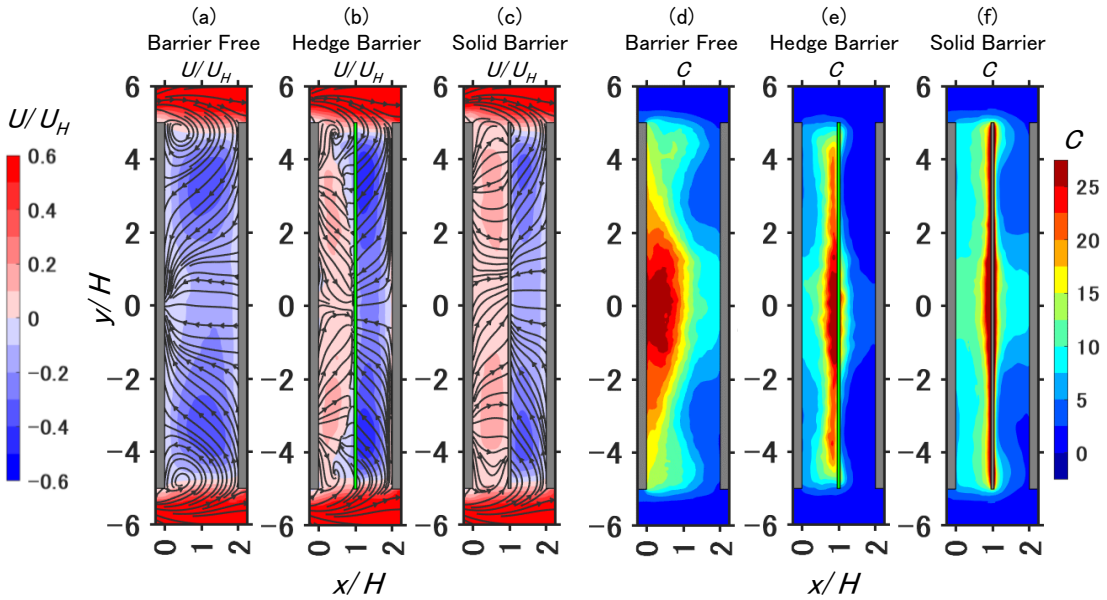


Fig. B1. Distributions of the time-averaged streamlines, streamwise velocity $U/U_H$ and concentration $C$ in the horizontal plane ($z/H$=0.08). The wind direction was perpendicular (90 degrees) to the street.

Fig. B1 shows the time-averaged streamlines, streamwise velocity and concentration in the whole horizontal plane ($z/H$=0.08) in the street canyon. The wind direction was perpendicular (90 degrees) to the street. As the sampling time was sufficient, the distributions were almost symmetric in the $y$-direction. For simplicity, the simulation results under perpendicular wind direction in Section 3 were averaged at mirror-symmetric locations and only half-side results were presented.